Exploring the Dynamical Interplay between Mass-Energy Equivalence, Interactions, and Entanglement in an Optical Lattice Clock

Anjun Chu,[1,2,*] Victor J. Martínez-Lahuerta,[3] Maya Miklos,[1] Kyungtae Kim,[1] Peter Zoller,[4,5] Klemens Hammerer,[3] Jun Ye,[1] and Ana Maria Rey[1,2]

[1]JILA, NIST, and Department of Physics, University of Colorado, Boulder, Colorado 80309, USA
[2]Center for Theory of Quantum Matter, University of Colorado, Boulder, Colorado 80309, USA
[3]Institut für Theoretische Physik, Leibniz Universität Hannover, Appelstraße 2, 30167 Hannover, Germany
[4]Institute for Quantum Optics and Quantum Information of the Austrian Academy of Sciences, 6020 Innsbruck, Austria
[5]Institute for Theoretical Physics, University of Innsbruck, 6020 Innsbruck, Austria

(Received 13 June 2024; revised 24 October 2024; accepted 17 January 2025; published 3 March 2025)

We propose protocols that probe manifestations of the mass-energy equivalence in an optical lattice clock interrogated with spin coherent and entangled quantum states. To tune and uniquely distinguish the mass-energy equivalence effects (gravitational redshift and second-order Doppler shift) in such a setting, we devise a dressing protocol using an additional nuclear spin state. We then analyze the dynamical interplay between photon-mediated interactions and gravitational redshift and show that such interplay can lead to entanglement generation and frequency synchronization dynamics. In the regime where all atomic spins synchronize, we show the synchronization time depends on the initial entanglement of the state and can be used as a proxy of its metrological gain compared to a classical state. Our work opens new possibilities for exploring the effects of general relativity on quantum coherence and entanglement in optical lattice clock experiments.

DOI: 10.1103/PhysRevLett.134.093201

Introduction—Understanding the interplay between quantum mechanics and general relativity (GR) is a fundamental quest for modern science. Nevertheless, to date measurements capable of genuinely witnessing this simultaneous interplay have not been realized in tabletop experiments. A push forward toward this milestone is becoming feasible thanks to recent improvements in the precision and accuracy of atomic clocks and interferometers. For example, matter-wave interferometers have been used for stringent tests on the equivalence principle [1–4]. In parallel, the resolution of the gravitational redshift using spatially separated clocks has improved from meter scales [5,6] to submillimeter [7,8]. Furthermore, coherence times for both clocks and matter-wave interferometers are now sufficiently long [7,9] to consider integrating clocks and interferometers on a single platform. These developments open up unique opportunities to search for new physics [1,10] that could help reconcile the seemingly contradictory predictions of quantum mechanics and GR.

Experimental developments have in parallel driven a great deal of theoretical effort toward the understanding of quantum dynamics with GR corrections. These progresses encompass analyses of relativistic corrections to Hamiltonians considered specifically in the context of neutral-atom and trapped-ion systems [11–22]; tests of mass-energy equivalence with atoms in internal superposition states, including predictions of energy-dependent phase shifts; loss of coherence; and spin-motion coupling induced by gravitational time dilation [23–31], among others [32–38]. However, understanding the direct consequence of GR effects in more complex scenarios such as many-body systems, where particles can interact over the entire array, remains an outstanding problem.

In this Letter, we provide a first step in this direction by proposing near-term protocols to explore manifestations of single-atom GR effects, including the gravitational redshift (GRS) and the second-order Doppler shift (SDS), in the quantum many-body dynamics of an atomic ensemble. We take advantage of the state-of-the-art Wannier-Stark optical lattice clocks (OLCs) that interrogate large arrays of interacting particles under gravity [7,39]. We analyze the GRS and the SDS specifically in Wannier-Stark OLCs, both governed by the same mechanism known as mass-energy equivalence. To distinctly characterize these GR effects and overcome the limitation that the gravitational redshift acts just as an effective magnetic field gradient in current OLCs, we *first* devise a dressing protocol using an additional nuclear spin state to tune and uniquely distinguish the mass-energy equivalence. *Second*, we propose a spectroscopic protocol to probe the dynamical modification of the GRS due to photon-mediated interactions in the array. Depending on the relative strength of the GRS to the photon-mediated interactions, the atomic

*Contact author: anjun.chu@colorado.edu

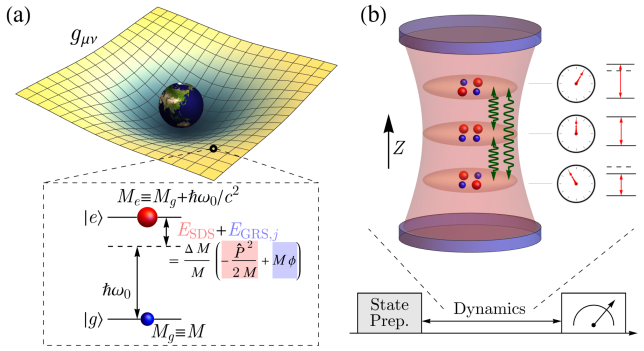

FIG. 1. (a) Schematic of an optical lattice clock embedded in the curved spacetime (metric $g_{\mu\nu}$) formed by the Earth's gravity. Mass-energy equivalence is the leading order GR correction that translates internal energy difference $\hbar\omega_0$ between $|e\rangle$ and $|g\rangle$ states into a difference in the rest mass of an atom $\hbar\omega_0/c^2$. Such type of correction generates second-order Doppler shift E_{SDS} and gravitational redshift $E_{\mathrm{GRS},j}$ to the clock transition [see Eqs. (3) and (4)]. (b) Schematic of probing the dynamical interplay between gravitational redshift and collective cavity-mediated interactions [see Eq. (5)].

phases dynamically evolve from their individual values, dictated by the local GRS, into a semilocal or global synchronized regime. In both cases we observe entanglement growth from an initial product state due to the interplay of the GRS and interactions, in contrast to the entanglement generated directly by gravitational interactions between massive objects [32,33,36–38]. *Last*, we analyze the interplay of the GRS and interactions when they act on an initially entangled state. This is achieved by studying the dependence of the global synchronization time on the entanglement content of the initial state. Remarkably we find the synchronization time can be used as a probe of the state's metrological utility.

Mass-energy equivalence in OLCs—We consider a single atom in Earth's gravity described by a curved spacetime metric $g_{\mu\nu}$ [see Fig. 1(a)]. We perform an expansion of $g_{\mu\nu}$ in a power series of ϕ/c^2 [40,41], with $\phi(Z) \approx g_{\mathrm{LO}} Z$ the Newtonian gravitational potential near the Earth's surface and g_{LO} the local gravitational acceleration. Following the treatment in Refs. [11,14,16,18], one can obtain a single-atom Hamiltonian $\hat{H}_A$ accounting for the leading relativistic corrections,

$$\hat{H}_A = \hat{H}_{\mathrm{point}}\left(M + \frac{\hat{H}_I}{c^2}\right) + O(c^{-4}). \tag{1}$$

Here, $\hat{H}_{\mathrm{point}}(M) = Mc^2 + \hat{H}_0(M) + \hat{H}_{\mathrm{other}}$ is the Hamiltonian of a point particle with mass M, $\hat{H}_0(M) = \hat{\mathbf{P}}^2/(2M) + M\phi$ contains the nonrelativistic terms, and $\hat{H}_{\mathrm{other}}$ contains other GR corrections in center-of-mass coordinates negligible in our case (see [41]). The key idea of Eq. (1) can be understood as the mass-energy equivalence, summarized by the replacement $M \to M + \hat{H}_I/c^2$ in $\hat{H}_{\mathrm{point}}$. OLCs feature an ultranarrow optical transition (clock transition) between two long-lived electronic states (excited state $|e\rangle$, ground state $|g\rangle$), which is described by the internal Hamiltonian $\hat{H}_I = \hbar\omega_0|e\rangle\langle e|$, with ω_0 the clock transition frequency measured at the lab position $Z = 0$ [see Fig. 1(a)]. Since in an OLC $\hat{H}_I$ contains the largest observable energy scale compared to other terms, the mass-energy equivalence is the leading order GR correction. It translates into a difference in the rest mass of an atom in states $|e\rangle$ and $|g\rangle$: $M_g = M$, $\Delta M_0 = M_e - M_g = \hbar\omega_0/c^2$. Note that in general the mass defect $\Delta M = \langle \hat{H}_I \rangle/c^2$ is not simply a fixed number, and its tunability (see Fig. 2) is an important tool to determine the relativistic origin of the mass defect.

We assume that in OLCs atoms are trapped in a magic-wavelength 1D lattice along the gravitational potential (Z axis) [7,39], where $|e\rangle$ and $|g\rangle$ states experience the same potential, $V(Z) = V_Z \sin^2(k_L Z) + M\phi$. Here, V_Z is the lattice depth, k_L is the wave number of the lattice that sets the atomic recoil energy $E_R = \hbar^2 k_L^2/2M$ and lattice spacing $a_L = \pi/k_L$. GR corrections to the optical lattice potential are negligible in our case (see [41]). In a tilted 1D lattice described by $V(Z)$, the motional eigenstates in the ground band are the so-called Wannier-Stark (WS) states $|W_j\rangle$, with j the Z-lattice site index where the WS state is centered [39]. Assuming the radial degrees of freedom are also confined to the lowest ground state by an additional 2D lattice, with lattice depths $V_{X,Y}$, the eigenenergies of WS states are given by $E_j = Mg_{\mathrm{LO}}a_L j + E_{\mathrm{band}}$, where $E_{\mathrm{band}} \approx \sum_{\alpha=X,Y,Z} E_R(\sqrt{V_\alpha/E_R} - 1/4)$ [48] is the ground band zero-point energy. The GR corrections due to mass-energy equivalence is given by

$$\hat{H}_{\mathrm{corr}} = \sum_j (E_{\mathrm{GRS},j} + E_{\mathrm{SDS}})|e, W_j\rangle\langle e, W_j|, \tag{2}$$

with $E_{\mathrm{GRS},j}$ the gravitational redshift (GRS) and E_{SDS} the second-order Doppler shift (SDS). Their orders of magnitude are discussed below for ^{87}Sr atoms.

Applying the mass-energy equivalence to the gravitational potential energy $M\phi$, we get the GRS (or gravitational time dilation) between $|e\rangle$ and $|g\rangle$ states ($\Delta M = \Delta M_0$),

$$E_{\mathrm{GRS},j} = \frac{\Delta M}{M}\langle W_j|M\phi|W_j\rangle = \hbar\omega_0 \frac{g_{\mathrm{LO}} a_L j}{c^2}. \tag{3}$$

The GRS leads to a gradient of frequency shifts across the lattice. For example, the fractional frequency difference for nearest-neighbor lattice sites is just 4.4×10^{-23}, while it is at the order of 10^{-19} for 1 mm spatial separation as recently observed [7,8].

The contribution of mass-energy equivalence in the kinetic energy leads to a local modification of the zero-

point energy known as SDS (or motional time dilation in special relativity) between $|e\rangle$ and $|g\rangle$ states,

$$E_{\mathrm{SDS}} = -\frac{\Delta M}{M}\frac{\langle W_j|\hat{\mathbf{P}}^2|W_j\rangle}{2M} = -\frac{\hbar\omega_0}{2Mc^2}E_{\mathrm{band}}. \quad (4)$$

The magnitude of E_{SDS} increases with the lattice depth. For example, a deep lattice with $V_{X,Y,Z} = 300E_R$ leads to the fractional frequency shift -4.5×10^{-21}. Corrections in the kinetic energy can also lead to a modification of the WS wave functions for $|e\rangle$ atoms, while they play a negligible role compared to $E_{\mathrm{GRS},j}$ and E_{SDS}.

Tuning and distinguishing GR effects—In standard OLCs, the effects of GRS might be mimicked by a weak magnetic field gradient. To provide further evidence of genuine GR effects beyond ruling out all possible systematics, one approach is to simultaneously observe $E_{\mathrm{GRS},j}$ and E_{SDS} in the same system. This could be achieved in next-term OLCs by populating higher motional bands if the systematic uncertainty of lattice Stark shifts [49] is suppressed below 10^{-20}.

An alternative approach is to use dressed states as a means to tune the mass defect ΔM and with it simultaneously change $E_{\mathrm{GRS},j}$ and E_{SDS}. As shown in Fig. 2(a), we make use of the intrinsic multilevel structure in fermionic alkaline earth atoms with nuclear spin F. We apply a dressing beam with Rabi frequency Ω and detuning δ connecting $|e, m_F\rangle$ with $|g, m_F - 1\rangle$ states, leading to the dressed states, $|+\rangle = C_1|e, m_F\rangle + C_2|g, m_F - 1\rangle$, $|-\rangle = -C_2|e, m_F\rangle + C_1|g, m_F - 1\rangle$, with $C_1 = (1 - \delta/\sqrt{\Omega^2 + \delta^2})^{1/2}/\sqrt{2}$, $C_2 = (1 + \delta/\sqrt{\Omega^2 + \delta^2})^{1/2}/\sqrt{2}$ in the rotating frame of the dressing laser (see End Matter). By addressing the transition between $|\uparrow\rangle \equiv |-\rangle$ and $|\downarrow\rangle \equiv |g, m_F\rangle$ states with a clock laser for the $\Delta m_F = 0$ transition, one can therefore get a tunable mass defect $\Delta M = |C_2|^2\Delta M_0$ in the dressed clock transition via scanning the dressing parameter δ/Ω [see Fig. 2(b)]. Since the nuclear spin states in the ground manifold share the same mass M but different Zeeman shifts, the dressing allows us to differentiate between a gravitational redshift and a magnetic field gradient. In the lab frame, we can understand the tunability of the mass-energy equivalence achieved by the dressing scheme by noticing that the state $|-\rangle$ has a probability $|C_2|^2$ to be in the $|e\rangle$ level and therefore an average internal energy of $|C_2|^2\hbar\omega_0$.

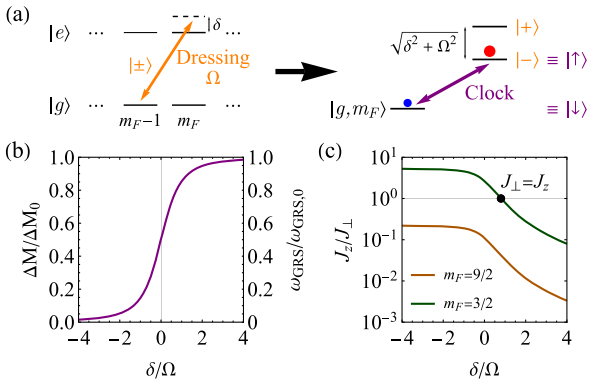

FIG. 2. Tuning mass-energy equivalence via dressed states. (a) Schematic of dressing the clock transition with another nuclear spin. The left panel shows the application of the dressing laser, and the right panel shows the new clock transition in the dressed basis. (b) The tunability of the mass defect ΔM and gravitational redshift ω_{GRS} as a function of dressing parameter δ/Ω. ΔM_0 and $\omega_{\mathrm{GRS},0}$ are the corresponding values without dressing. (c) The tunability of cavity-mediated interactions [see $\hat{H}_{\mathrm{cGR}}$ in Eq. (5)] as a function of dressing parameters δ/Ω and nuclear spin level m_F. The Heisenberg interaction ($J_\perp = J_z$) can be reached with $m_F = 3/2$.

This protocol is feasible thanks to the fact that the clock transitions between different nuclear spins are frequency resolved due to magnetic Zeeman shifts. We also assume all other dynamical frequencies are smaller than the dressed state energy gap $\sqrt{\Omega^2 + \delta^2}$ and the Zeeman shifts between nuclear spins. To guarantee the matching of laser phases for each atom, the dressing beam and the clock beam should be copropagating. Moreover, spatial inhomogeneities in atomic detunings δ and in the dressing laser Rabi frequency Ω might obscure the effects of gravitational redshift. For a mHz gravitational redshift arising from a cm-scale spatial separation, the spatial variations of $\delta(Z)$, $\Omega(Z)$, and other source of perturbations need to be suppressed below 10^{-4} Hz. The requirement for $\delta(Z)$ is attainable based on the parameters in Ref. [7]. The requirement for $\Omega(Z)$ could be achievable using a cavity to stabilize the spatial mode of the dressing laser. One can also circumvent the stringent requirement for $\Omega(Z)$ by averaging the transition frequency of $|g, m_F\rangle \leftrightarrow |-\rangle$ and $|g, m_F\rangle \leftrightarrow |+\rangle$ (see End Matter), while sacrificing the tunability of mass defect ($\Delta M = \Delta M_0/2$).

Many-body dynamics—After providing a recipe to distinguish genuine GR effects in OLCs, we further explore their manifestations in quantum many-body dynamics. We consider photon-mediated interactions generated by placing the atoms in an optical cavity [42,50], in a regime where atomic contact interactions are controlled to be much weaker. The interplay between photon-mediated interactions and the GRS is described by the following Hamiltonian [see Fig. 1(b) and End Matter]:

$$\hat{H}_{\mathrm{cGR}}/\hbar = J_\perp\hat{\mathbf{S}}\cdot\hat{\mathbf{S}} + (J_z - J_\perp)\hat{S}^z\hat{S}^z + \omega_{\mathrm{GRS}}\sum_j j\hat{\mathcal{S}}^z_j, \quad (5)$$

where $\hbar\omega_{\mathrm{GRS}} = (\Delta M)g_{\mathrm{LO}}a_L$ is the GRS between nearest-neighbor sites, $J_\perp$ and J_z are the collective exchange and Ising couplings. Here, $\hat{\mathcal{S}}^{x,y,z}_j$ are collective spin operators summed over all atoms at the same height ja_L, and $\hat{S}^{x,y,z} = \sum_j \hat{\mathcal{S}}^{x,y,z}_j$. Based on Eq. (5), a magnetic field gradient will in principle give rise to similar single-atom inhomogeneities in the Hamiltonian, but we can tell them

apart using the dressing scheme. We drop the GR corrections for interaction terms since they are negligible in our case (see [41]). While the use of a single nuclear spin state restricts the cavity exchange interactions to a single polarization mode ($J_z = 0$ only), the dressing to another nuclear spin allows for coupling two polarization modes of the cavity (see End Matter), which enhances the tunability of $\hat{H}_{\mathrm{cGR}}$ and realizes collective Heisenberg interactions ($J_\perp = J_z$) as shown in Fig. 2(c). In the following, we mainly focus on the case of $J_\perp = J_z$, since the $\hat{\mathbf{S}} \cdot \hat{\mathbf{S}}$ term becomes a constant and does not alter entanglement in the fully symmetric manifold. This requirement is unnecessary for observing frequency synchronization.

We propose to initialize all the atoms in the state $(|\uparrow\rangle + |\downarrow\rangle)/\sqrt{2}$ ($\pi/2$ pulse between the dressed clock levels), perform time evolution under Hamiltonian $\hat{H}_{\mathrm{cGR}}$ [Eq. (5)], and then measure the phase shift of $\langle \hat{S}_j^+ \rangle$ for every Z-lattice site, resulting in frequency shift $\omega_j(t) = \tan^{-1}\left[\langle \hat{S}_j^y \rangle / \langle \hat{S}_j^x \rangle\right]/t$ as a function of evolution time [see Fig. 3(a)]. It can be observed by the application of a $\pi/2$ pulse followed by local population measurements. Without interactions or in the case of short interrogation times, one expects to observe the GRS, $\omega_j = j\omega_{\mathrm{GRS}}$, as reported in Ref. [7]. In the interaction dominated regime, the GRS persists only for a timescale shorter than the atomic interaction timescale. Beyond this period, the frequencies become synchronized due to interaction locking and reach $\omega_j \approx 0$ at synchronization time t_{syn} [see Fig. 3(b)]. Without loss of generality, the numerical simulations in Figs. 3 and 4 are based on exact diagonalization for $N = 16$ atoms with one atom per Z-lattice site.

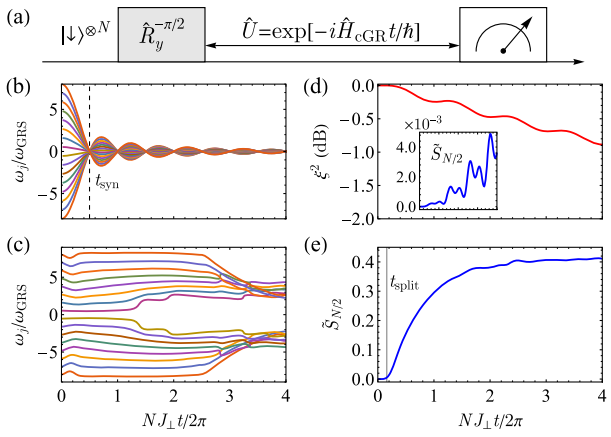

FIG. 3. Interplay between photon-mediated interactions and GRS. (a) We prepare a product state with all atoms in $|\downarrow\rangle$ state and apply a laser pulse $\hat{R}_y^{-\pi/2} = \exp[i(\pi/2)\hat{S}^y]$ to start the dynamics. We focus on a single chain with $N = 16$ atoms under the Hamiltonian $\hat{H}_{\mathrm{cGR}}$ [Eq. (5)] with $J_\perp = J_z$. (b) Individual atomic frequency shift ω_j with $\omega_{\mathrm{split}}/NJ_\perp = 0.3125$. Synchronization of atomic frequencies can be reach at time t_{syn}. (c) Individual atomic frequency shift ω_j with $\omega_{\mathrm{split}}/NJ_\perp = 3.125$. Global synchronization fails to occur in this regime. (d) Spin squeezing parameter ξ^2 and normalized Rényi entropy $\tilde{S}_{N/2}$ (inset) in the case of (b). (e) Normalized Rényi entropy $\tilde{S}_{N/2}$ in the case of (c). Entanglement starts to build up at a timescale t_{split} in this case.

The emergent synchronization is the result of many-body gap protection also observed in prior experiments [42,51–55], which arises when $\omega_{\mathrm{split}} \ll \Delta E$. Here, $\omega_{\mathrm{split}} = (N_s - 1)\omega_{\mathrm{GRS}}$ is the maximum redshift in the array, with N_s the number of Z-lattice sites, and ΔE is the many-body gap due to Heisenberg couplings. On the contrary, in the regime $\omega_{\mathrm{split}} \sim \Delta E$, the gap cannot maintain global synchronization [see Fig. 3(c)]. Using a spin wave analysis one obtains $\Delta E = NJ_\perp$ and $NJ_\perp t_{\mathrm{syn}} = \pi$ for $J_\perp = J_z$, where N corresponds to the total atom number in the array [41]. For $N \sim 10^5$ ^{87}Sr atoms, one can achieve $NJ_\perp/2\pi \sim$ Hz ($\omega_{\mathrm{split}}/NJ_\perp \sim 10^{-3}$ for cm-scale separation) [42], leading to a synchronization timescale (∼1 s) within reach of current experiments.

Furthermore, we find that the simultaneous presence of single-atom GRS and photon-mediated interactions can lead to quantum entanglement as shown in Figs. 3(d) and 3(e). In fact, in the regime $\omega_{\mathrm{split}} \ll \Delta E$, the projection of the wave function into the fully symmetric manifold imposed by the many-body gap transforms the single-particle term into an effective one-axis twisting (OAT) [56,57] interaction term $\chi \hat{S}^z \hat{S}^z$, with $\chi \sim \omega_{\mathrm{split}}^2/[N(\Delta E)]$ (see Ref. [58] where the splitting is generated by a different mechanism). In this case, entanglement builds up for $t > t_{\mathrm{syn}}$, as witnessed by a squeezing parameter [57], $\xi^2 \equiv \min_\varphi N(\Delta S_\varphi^\perp)^2/|\langle \hat{\mathbf{S}} \rangle|^2 < 1$ [see Fig. 3(d)]. Here, $(\Delta S_\varphi^\perp)^2$ is the variance of spin noise along an axis perpendicular to the collective spin $\langle \hat{\mathbf{S}} \rangle$. A faster growth of entanglement can be seen in the regime $\omega_{\mathrm{split}} \sim \Delta E$ [see Fig. 3(e)]. Since the entanglement in this case is not captured by spin squeezing, instead we characterize the entanglement by the normalized Rényi entropy $\tilde{S}_{N/2} = -2\log_2[\mathrm{tr}(\hat{\rho}_{N/2}^2)]/N$, where $\hat{\rho}_{N/2}$ is the reduced density matrix by taking partial trace over half of the system. The entanglement builds up at a timescale $t_{\mathrm{split}} \sim \pi/\omega_{\mathrm{split}}$ in this case, which might be due to population transfer to highly entangled states in manifolds of lower total spin. For the implementation of entanglement generation, $\omega_{\mathrm{split}}/NJ_\perp \sim 0.1$–1 is achievable for 10 cm to 1 m separation and $NJ_\perp/2\pi \sim 0.1$ Hz. Therefore, the timescale for entanglement growth is at the order of 10 s and thus requires careful suppression of systematics.

To study the effects of the GRS on quantum entanglement, we consider the scenario with entangled initial states, such as the ones generated using cavity induced OAT interactions [59,60], $\hat{U}_{\mathrm{OAT}}(Q) = \exp(-iQ\hat{S}^z\hat{S}^z/N)$, where Q is the shearing strength [Fig. 4(a)]. The squeezing direction corresponds to the direction with minimum value of $(\Delta S_\varphi^\perp)^2$, which can be controlled by performing a

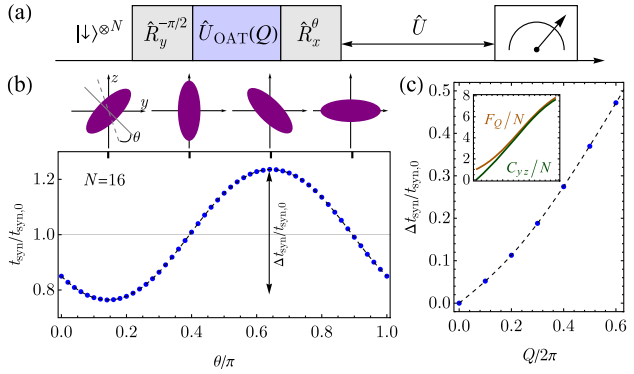

FIG. 4. Interplay between entanglement and GRS. (a) One-axis twisting (OAT) interactions $\hat{U}_{\rm OAT}(Q) = \exp(-iQ\hat{S}^z\hat{S}^z/N)$ and rotations $\hat{R}_x^{\theta} = \exp(-i\theta\hat{S}^x)$ are first applied to generate a spin squeezed initial state (at $Q/2\pi = 0.6$), followed by unitary evolution under $\hat{H}_{\rm cGR}$. (b) The synchronization time $t_{\rm syn}$ depends on the orientation of the spin squeezed state determined by θ. (c) $\Delta t_{\rm syn}$ [marked in (b)] as a function of OAT shearing strength Q. We show $C_{yz} = 4\max_\theta {\rm Cov}(y,z)$ is approaching the quantum Fisher information F_Q for spin squeezed states (inset). We compare the numerical simulations (blue points) for $N = 16$ atoms under $\hat{H}_{\rm cGR}$ ($J_\perp = J_z$) with Eq. (6) (black dashed lines).

rotation $\hat{R}_x^{\theta} = \exp(-i\theta\hat{S}^x)$ as shown in Fig. 4. As demonstrated in Ref. [60], entangled state preparation timescales in an OLC are at the order of 10 ms, so it is reasonable to ignore GRS in initial state preparation. We use $|\psi_0\rangle$ to denote the state after OAT interactions, and $|\psi(\theta)\rangle$ for the state after the $\hat{R}_x^{\theta}$ rotation.

In Fig. 4(b), we show that it is possible to control $t_{\rm syn}$ below or above the value of a product initial state $t_{\rm syn,0}$ ($Q = 0$, as obtained in Fig. 3) depending on the rotation $\hat{R}_x^{\theta}$. The ratio $t_{\rm syn}/t_{\rm syn,0}$ under $\hat{H}_{\rm cGR}$ ($J_\perp = J_z$) can be understood using the following analytic result [41]:

$$\frac{t_{\rm syn}}{t_{\rm syn,0}} = 1 - \frac{2}{\pi}\arctan\left[\frac{{\rm Cov}(y,z)}{(N-1)\langle\psi_0|\hat{S}^x|\psi_0\rangle}\right], \qquad (6)$$

where ${\rm Cov}(\alpha,\beta) \equiv \langle\psi(\theta)|(\hat{S}^\alpha\hat{S}^\beta + \hat{S}^\beta\hat{S}^\alpha)|\psi(\theta)\rangle - 2\langle\psi(\theta)|\hat{S}^\alpha|\psi(\theta)\rangle\langle\psi(\theta)|\hat{S}^\beta|\psi(\theta)\rangle$, with $\alpha,\beta = x, y, z$. The tunability of $t_{\rm syn}$ is due to the θ dependence of ${\rm Cov}(y,z)$. The tunable range $\Delta t_{\rm syn} \equiv \max_\theta t_{\rm syn} - \min_\theta t_{\rm syn}$ can be used as a measure of entanglement [see Fig. 4(c)], since $C_{yz} = 4\max_\theta {\rm Cov}(y,z)$ is approaching the quantum Fisher information F_Q [57], which corresponds to the maximal eigenvalue of the matrix $F_{Q,\alpha\beta} = 2{\rm Cov}(\alpha,\beta)$.

Conclusion and outlook—We discussed protocols accessible in OLCs that explore how the single-atom GR effects modify many-body dynamics generated by photon-mediated interactions. A similar interplay should be observable with atomic superexchange interactions. While so far we have mostly focused on highly localized atomic arrays, generalizations to the case of itinerant particles where motion and other GR corrections also become relevant, will open unique opportunities for testing the basic tenets of GR when extended into the complex quantum domain.

Acknowledgments—We thank James Thompson, Raphael Kaubruegger, Dylan Young, Alexander Aeppli, Michael Werner, and Torsten Zache for useful discussions. This work is supported by the Sloan Foundation, the Simons Foundation and the Heising-Simons Foundation, NSF JILA-PFC PHY-2317149 and NSF OMA-2016244 (QLCI) grants, and by NIST. V. M. L. and K. H. acknowledge funding by the Deutsche Forschungsgemeinschaft (DFG, German Research Foundation) through Project-ID 274200144 – SFB 1227 (project A09) and Project-ID 390837967 - EXC 2123.

[1] G. M. Tino, Testing gravity with cold atom interferometry: Results and prospects, Quantum Sci. Technol. **6**, 024014 (2021).
[2] S. Fray, C. A. Diez, T. W. Hänsch, and M. Weitz, Atomic interferometer with amplitude gratings of light and its applications to atom based tests of the equivalence principle, Phys. Rev. Lett. **93**, 240404 (2004).
[3] G. Rosi, G. D'Amico, L. Cacciapuoti, F. Sorrentino, M. Prevedelli, M. Zych, Č. Brukner, and G. M. Tino, Quantum test of the equivalence principle for atoms in coherent superposition of internal energy states, Nat. Commun. **8**, 15529 (2017).
[4] P. Asenbaum, C. Overstreet, M. Kim, J. Curti, and M. A. Kasevich, Atom-interferometric test of the equivalence principle at the 10^{-12} level, Phys. Rev. Lett. **125**, 191101 (2020).
[5] C.-W. Chou, D. B. Hume, T. Rosenband, and D. J. Wineland, Optical clocks and relativity, Science **329**, 1630 (2010).
[6] M. Takamoto, I. Ushijima, N. Ohmae, T. Yahagi, K. Kokado, H. Shinkai, and H. Katori, Test of general relativity by a pair of transportable optical lattice clocks, Nat. Photonics **14**, 411 (2020).
[7] T. Bothwell, C. J. Kennedy, A. Aeppli, D. Kedar, J. M. Robinson, E. Oelker, A. Staron, and J. Ye, Resolving the gravitational redshift across a millimetre-scale atomic sample, Nature (London) **602**, 420 (2022).
[8] X. Zheng, J. Dolde, M. C. Cambria, H. M. Lim, and S. Kolkowitz, A lab-based test of the gravitational redshift with a miniature clock network, Nat. Commun. **14**, 4886 (2023).
[9] V. Xu, M. Jaffe, C. D. Panda, S. L. Kristensen, L. W. Clark, and H. Müller, Probing gravity by holding atoms for 20 seconds, Science **366**, 745 (2019).
[10] M. S. Safronova, D. Budker, D. DeMille, D. F. J. Kimball, A. Derevianko, and C. W. Clark, Search for new physics with atoms and molecules, Rev. Mod. Phys. **90**, 025008 (2018).
[11] F. E. Close and H. Osborn, Relativistic center-of-mass motion and the electromagnetic interaction of systems of charged particles, Phys. Rev. D **2**, 2127 (1970).

[12] K.-P. Marzlin, Dipole coupling of atoms and light in gravitational fields, Phys. Rev. A **51**, 625 (1995).
[13] S. Dimopoulos, P. W. Graham, J. M. Hogan, and M. A. Kasevich, General relativistic effects in atom interferometry, Phys. Rev. D **78**, 042003 (2008).
[14] M. Sonnleitner and S. M. Barnett, Mass-energy and anomalous friction in quantum optics, Phys. Rev. A **98**, 042106 (2018).
[15] V. Yudin and A. Taichenachev, Mass defect effects in atomic clocks, Laser Phys. Lett. **15**, 035703 (2018).
[16] P. K. Schwartz and D. Giulini, Post-Newtonian Hamiltonian description of an atom in a weak gravitational field, Phys. Rev. A **100**, 052116 (2019).
[17] S. Khandelwal, M. P. E. Lock, and M. P. Woods, Universal quantum modifications to general relativistic time dilation in delocalised clocks, Quantum **4**, 309 (2020).
[18] V. J. Martínez-Lahuerta, S. Eilers, T. E. Mehlstäubler, P. O. Schmidt, and K. Hammerer, *Ab initio* quantum theory of mass defect and time dilation in trapped-ion optical clocks, Phys. Rev. A **106**, 032803 (2022).
[19] F. Di Pumpo, C. Ufrecht, A. Friedrich, E. Giese, W. P. Schleich, and W. G. Unruh, Gravitational redshift tests with atomic clocks and atom interferometers, PRX Quantum **2**, 040333 (2021).
[20] P. T. Grochowski, A. R. H. Smith, A. Dragan, and K. Dębski, Quantum time dilation in atomic spectra, Phys. Rev. Res. **3**, 023053 (2021).
[21] F. Di Pumpo, A. Friedrich, A. Geyer, C. Ufrecht, and E. Giese, Light propagation and atom interferometry in gravity and dilaton fields, Phys. Rev. D **105**, 084065 (2022).
[22] M. Werner, P. K. Schwartz, J.-N. Kirsten-Siemß, N. Gaaloul, D. Giulini, and K. Hammerer, Atom interferometers in weakly curved spacetimes using bragg diffraction and bloch oscillations, Phys. Rev. D **109**, 022008 (2024).
[23] M. Zych, F. Costa, I. Pikovski, and Č. Brukner, Quantum interferometric visibility as a witness of general relativistic proper time, Nat. Commun. **2**, 505 (2011).
[24] I. Pikovski, M. Zych, F. Costa, and Č. Brukner, Universal decoherence due to gravitational time dilation, Nat. Phys. **11**, 668 (2015).
[25] I. Pikovski, M. Zych, F. Costa, and Č. Brukner, Time dilation in quantum systems and decoherence, New J. Phys. **19**, 025011 (2017).
[26] M. Zych and Č. Brukner, Quantum formulation of the Einstein equivalence principle, Nat. Phys. **14**, 1027 (2018).
[27] R. Haustein, G. J. Milburn, and M. Zych, Mass-energy equivalence in harmonically trapped particles, arXiv:1906.03980.
[28] A. Roura, Gravitational redshift in quantum-clock interferometry, Phys. Rev. X **10**, 021014 (2020).
[29] A. R. H. Smith and M. Ahmadi, Quantum clocks observe classical and quantum time dilation, Nat. Commun. **11**, 5360 (2020).
[30] G. Tobar, S. Haine, F. Costa, and M. Zych, Mass-energy equivalence in gravitationally bound quantum states of the neutron, Phys. Rev. A **106**, 052801 (2022).
[31] T. Asano, E. Giese, and F. Di Pumpo, Quantum field theory for multipolar composite bosons with mass defect and relativistic corrections, PRX Quantum **5**, 020322 (2024).
[32] C. Marletto and V. Vedral, Gravitationally induced entanglement between two massive particles is sufficient evidence of quantum effects in gravity, Phys. Rev. Lett. **119**, 240402 (2017).
[33] S. Bose, A. Mazumdar, G. W. Morley, H. Ulbricht, M. Toroš, M. Paternostro, A. A. Geraci, P. F. Barker, M. S. Kim, and G. Milburn, Spin entanglement witness for quantum gravity, Phys. Rev. Lett. **119**, 240401 (2017).
[34] M. Zych, Ł. Rudnicki, and I. Pikovski, Gravitational mass of composite systems, Phys. Rev. D **99**, 104029 (2019).
[35] A. J. Paige, A. D. K. Plato, and M. S. Kim, Classical and nonclassical time dilation for quantum clocks, Phys. Rev. Lett. **124**, 160602 (2020).
[36] D. Carney, H. Müller, and J. M. Taylor, Using an atom interferometer to infer gravitational entanglement generation, PRX Quantum **2**, 030330 (2021).
[37] J. S. Pedernales, K. Streltsov, and M. B. Plenio, Enhancing gravitational interaction between quantum systems by a massive mediator, Phys. Rev. Lett. **128**, 110401 (2022).
[38] M. Christodoulou, A. Di Biagio, M. Aspelmeyer, Č. Brukner, C. Rovelli, and R. Howl, Locally mediated entanglement in linearized quantum gravity, Phys. Rev. Lett. **130**, 100202 (2023).
[39] A. Aeppli, A. Chu, T. Bothwell, C. J. Kennedy, D. Kedar, P. He, A. M. Rey, and J. Ye, Hamiltonian engineering of spin-orbit-coupled fermions in a Wannier-Stark optical lattice clock, Sci. Adv. **8**, eadc9242 (2022).
[40] C. M. Will, *Theory and Experiment in Gravitational Physics* (Cambridge University Press, Cambridge, England, 2018).
[41] See Supplemental Material at http://link.aps.org/supplemental/10.1103/PhysRevLett.134.093201 for details of GR corrections in an OLC, additional numerical simulations of superexchange interactions, and analytical derivation of synchronization time, which includes Refs. [14,16,18,22,40,42–47].
[42] M. A. Norcia, R. J. Lewis-Swan, J. R. Cline, B. Zhu, A. M. Rey, and J. K. Thompson, Cavity-mediated collective spin-exchange interactions in a strontium superradiant laser, Science **361**, 259 (2018).
[43] L. Parker, One-electron atom as a probe of spacetime curvature, Phys. Rev. D **22**, 1922 (1980).
[44] L. Parker and L. O. Pimentel, Gravitational perturbation of the hydrogen spectrum, Phys. Rev. D **25**, 3180 (1982).
[45] Z.-H. Zhao, Y.-X. Liu, and X.-G. Lee, Energy-level shifts of a stationary hydrogen atom in a static external gravitational field with Schwarzschild geometry, Phys. Rev. D **76**, 064016 (2007).
[46] T. R. Perche and J. Neuser, A wavefunction description for a localized quantum particle in curved spacetimes, Classical Quantum Gravity **38**, 175002 (2021).
[47] A. Alibabaei, P. K. Schwartz, and D. Giulini, Geometric post-Newtonian description of massive spin-half particles in curved spacetime, Classical Quantum Gravity **40**, 235014 (2023).
[48] D. Jaksch, C. Bruder, J. I. Cirac, C. W. Gardiner, and P. Zoller, Cold bosonic atoms in optical lattices, Phys. Rev. Lett. **81**, 3108 (1998).

[49] K. Kim, A. Aeppli, T. Bothwell, and J. Ye, Evaluation of lattice light shift at low 10^{-19} uncertainty for a shallow lattice Sr optical clock, Phys. Rev. Lett. **130**, 113203 (2023).
[50] J. M. Robinson, M. Miklos, Y. M. Tso, C. J. Kennedy, T. Bothwell, D. Kedar, J. K. Thompson, and J. Ye, Direct comparison of two spin-squeezed optical clock ensembles at the 10^{-17} level, Nat. Phys. **20**, 208 (2024).
[51] J. C. Allred, R. N. Lyman, T. W. Kornack, and M. V. Romalis, High-sensitivity atomic magnetometer unaffected by spin-exchange relaxation, Phys. Rev. Lett. **89**, 130801 (2002).
[52] C. Deutsch, F. Ramirez-Martinez, C. Lacroûte, F. Reinhard, T. Schneider, J. N. Fuchs, F. Piéchon, F. Laloë, J. Reichel, and P. Rosenbusch, Spin self-rephasing and very long coherence times in a trapped atomic ensemble, Phys. Rev. Lett. **105**, 020401 (2010).
[53] S. Smale, P. He, B. A. Olsen, K. G. Jackson, H. Sharum, S. Trotzky, J. Marino, A. M. Rey, and J. H. Thywissen, Observation of a transition between dynamical phases in a quantum degenerate Fermi gas, Sci. Adv. **5**, eaax1568 (2019).
[54] E. J. Davis, A. Periwal, E. S. Cooper, G. Bentsen, S. J. Evered, K. Van Kirk, and M. H. Schleier-Smith, Protecting spin coherence in a tunable Heisenberg model, Phys. Rev. Lett. **125**, 060402 (2020).
[55] D. J. Young, A. Chu, E. Y. Song, D. Barberena, D. Wellnitz, Z. Niu, V. M. Schäfer, R. J. Lewis-Swan, A. M. Rey, and J. K. Thompson, Observing dynamical phases of BCS superconductors in a cavity QED simulator, Nature (London) **625**, 679 (2024).
[56] M. Kitagawa and M. Ueda, Squeezed spin states, Phys. Rev. A **47**, 5138 (1993).
[57] J. Ma, X. Wang, C.-P. Sun, and F. Nori, Quantum spin squeezing, Phys. Rep. **509**, 89 (2011).
[58] P. He, M. A. Perlin, S. R. Muleady, R. J. Lewis-Swan, R. B. Hutson, J. Ye, and A. M. Rey, Engineering spin squeezing in a 3d optical lattice with interacting spin-orbit-coupled fermions, Phys. Rev. Res. **1**, 033075 (2019).
[59] I. D. Leroux, M. H. Schleier-Smith, and V. Vuletić, Implementation of cavity squeezing of a collective atomic spin, Phys. Rev. Lett. **104**, 073602 (2010).
[60] E. Pedrozo-Peñafiel, S. Colombo, C. Shu, A. F. Adiyatullin, Z. Li, E. Mendez, B. Braverman, A. Kawasaki, D. Akamatsu, Y. Xiao *et al.*, Entanglement on an optical atomic-clock transition, Nature (London) **588**, 414 (2020).
[61] A. Piñeiro Orioli, J. K. Thompson, and A. M. Rey, Emergent dark states from superradiant dynamics in multilevel atoms in a cavity, Phys. Rev. X **12**, 011054 (2022).
[62] A. Chu, A. Piñeiro Orioli, D. Barberena, J. K. Thompson, and A. M. Rey, Photon-mediated correlated hopping in a synthetic ladder, Phys. Rev. Res. **5**, L022034 (2023).

End Matter

Construction of dressed states—Here, we explain the dressing scheme in Fig. 2 in more detail. Because of magnetic Zeeman shifts, the clock transitions between different nuclear spins are frequency resolved; thus we can restrict the dynamics within three internal levels $|e, m_F\rangle$, $|g, m_F\rangle$, and $|g, m_F - 1\rangle$. A dressing laser (with Rabi frequency Ω, laser frequency ω_d) is used to couple $|e, m_F\rangle$ with $|g, m_F - 1\rangle$ states [see Fig. 2(a)], leading to the following Hamiltonian:

$$\hat{H}_{\text{dress}}/\hbar = \omega_0 \hat{\mathcal{P}}_{e,m_F} - \omega_Z \hat{\mathcal{P}}_{g,m_F-1} + \frac{\Omega}{2}(|e, m_F\rangle\langle g, m_F - 1|e^{-i\omega_d t} + \text{H.c.}), \quad \text{(A1)}$$

where ω_Z is the Zeeman shift between $|g, m_F\rangle$ and $|g, m_F - 1\rangle$ states, and we set the energy of $|g, m_F\rangle$ state to 0. The projection operators are defined by $\hat{\mathcal{P}}_\psi = |\psi\rangle\langle\psi|$. We then perform a unitary transformation $\hat{U} = \exp(-i\omega_d t \hat{\mathcal{P}}_{g,m_F-1})$ to rewrite the Hamiltonian in the rotating frame of the dressing laser,

$$\hat{H}'_{\text{dress}}/\hbar = \omega_0 \hat{\mathcal{P}}_{e,m_F} + (\omega_0 + \delta)\hat{\mathcal{P}}_{g,m_F-1} + \frac{\Omega}{2}(|e, m_F\rangle\langle g, m_F - 1| + \text{H.c.}), \quad \text{(A2)}$$

where $\delta = \omega_d - \omega_0 - \omega_Z$ is the detuning of the dressing laser. The eigenstates of this Hamiltonian are given by $|+\rangle = C_1|e, m_F\rangle + C_2|g, m_F - 1\rangle$, $|-\rangle = -C_2|e, m_F\rangle + C_1|g, m_F - 1\rangle$ with energy $E_\pm/\hbar = \omega_0 + \delta/2 \pm \sqrt{\Omega^2 + \delta^2}/2$. These are the dressed states defined in the main text with coefficients $C_1 = (1 - \delta/\sqrt{\Omega^2 + \delta^2})^{1/2}/\sqrt{2}$ and $C_2 = (1 + \delta/\sqrt{\Omega^2 + \delta^2})^{1/2}/\sqrt{2}$.

Tunability of GR effects—We first analyze the effects of the dressing scheme on the GR effects. We focus on the GRS described by the following Hamiltonian:

$$\hat{H}_{\text{GRS}} = (\Delta M_0)\phi\hat{\mathcal{P}}_{e,m_F} = (\Delta M_0)\phi\big(|C_2|^2\hat{\mathcal{P}}_- + |C_1|^2\hat{\mathcal{P}}_+ + \big(C_1C_2^*|+\rangle\langle -| + \text{H.c.}\big)\big), \quad \text{(A3)}$$

where $\Delta M_0 = \hbar\omega_0/c^2$ is the mass defect without the dressing protocol. As shown in Fig. 2(a), we probe the transition between $|g, m_F\rangle$ and $|-\rangle$. Consider the case that the energy gap $\sqrt{\Omega^2 + \delta^2}$ between $|+\rangle$ and $|-\rangle$ states due to $\hat{H}_{\text{dress}}$ is much larger than $\omega_0\phi/c^2$, the coupling between $|+\rangle$ and $|-\rangle$ states in $\hat{H}_{\text{GRS}}$ are suppressed significantly. Therefore, to the leading order, when projected into the relevant $|g, m_F\rangle$ and $|-\rangle$ states we can write $\hat{H}_{\text{GRS}}$ as

$$\hat{H}_{\text{GRS}} \approx (\Delta M_0)\phi|C_2|^2\hat{\mathcal{P}}_- = (\Delta M)\phi\hat{\mathcal{P}}_-, \quad \text{(A4)}$$

which is equivalent to a modification of the mass defect [see Fig. 2(b)],

$$\Delta M = |C_2|^2 \Delta M_0. \tag{A5}$$

The same analysis applies to the SDS.

The tunability of gravitational redshift due to the dressing scheme allows us to distinguish GRS from a magnetic field gradient. In the dressing scheme, $\hat{H}_{\mathrm{GRS}}$ leads to a position-dependent correction of the dressed state energy E_-,

$$E_-(Z) = E_- + \frac{\hbar\omega_0 g_{\mathrm{LO}}}{c^2}|C_2|^2 Z, \tag{A6}$$

which can be resolved via clock spectroscopy in the effective two level system formed by $|g, m_F\rangle$ and $|-\rangle$ states. While for a small magnetic field gradient term adding on top of a constant magnetic field, we have $\omega_0(Z) = \omega_0 + (\eta_e - \eta_g) m_F Z$, $\omega_Z(Z) = \omega_Z + \eta_g Z$, where $\eta_e = -\mathcal{G}_{^3P_0}\mu_B \partial_Z B$, $\eta_g = -\mathcal{G}_{^1S_0}\mu_B \partial_Z B$, with $\mathcal{G}_{^3P_0}$ and $\mathcal{G}_{^1S_0}$ representing the Landé g factors, and μ_B is the Bohr magneton. So the position-dependent correction due to magnetic field gradients is given by

$$E_-(Z) = E_- + \left[|C_2|^2(\eta_e - \eta_g)m_F - |C_1|^2\eta_g\right] Z. \tag{A7}$$

Since $\eta_g \neq 0$, we find different dependence by varying δ compared to the GRS [see Eq. (A6)]. The reason is that different ground-state nuclear spins have the same mass but different Zeeman shifts.

Tunability of cavity-mediated interactions—Next we analyze the effects of the dressing protocol on the cavity-mediated interactions. We focus on multilevel alkaline earth atoms with the quantization axis for nuclear spins perpendicular to the cavity axis (see Fig. 5). In this case, the two polarization modes supported by the cavity can drive the π transition and the linear combination of σ^+ and σ^- transitions, so we can define the multilevel raising operators for these two polarization modes, $\hat{\Pi}^+ = \sum_{jm} C_m^0 |e, m\rangle_j\langle g, m|$, $\hat{\Sigma}^+ = \sum_{jm}(i/\sqrt{2})(C_m^{-1}|e, m-1\rangle_j\langle g, m| + C_m^{+1}|e, m+1\rangle_j\langle g, m|)$, where j is the label of atoms, m is the label of nuclear spins, and $C_m^\sigma \equiv \langle F, m; 1, \sigma | F, m+\sigma\rangle$ are the Clebsch-Gordan coefficients. The photon-mediated exchange interactions for multilevel alkaline earth atoms take the following form [61,62]:

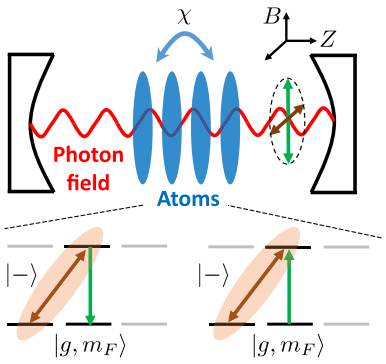

FIG. 5. Schematic of the cavity-mediated interactions in the dressed basis. The cavity axis is along Z and the quantization axis is along magnetic field B labeled in the plot. The additional nuclear spin state in the dressing protocol allows for coupling to two polarization modes in the cavity and enhancing the tunability of the cavity-mediated interactions.

$$\hat{H}_c/\hbar = \chi(\hat{\Pi}^+\hat{\Pi}^- + \hat{\Sigma}^+\hat{\Sigma}^-), \tag{A8}$$

with $\hat{\Pi}^- = (\hat{\Pi}^-)^\dagger$ and $\hat{\Sigma}^- = (\hat{\Sigma}^-)^\dagger$. Assuming the Zeeman shifts between nuclear spins and the energy gap $\sqrt{\Omega^2 + \delta^2}$ between two dressed states are typically larger than the interaction strength χN, one can restrict the dynamics within two levels, $|\downarrow\rangle \equiv |g, m_F\rangle$ and $|\uparrow\rangle \equiv |-\rangle$. We have

$$\hat{H}_c/\hbar \approx J_\perp \hat{S}^+\hat{S}^- + J_z\left(\frac{N}{2} + \hat{S}^z\right)^2, \tag{A9}$$

where

$$J_\perp = \chi(C_{m_F}^0)^2|C_2|^2, \quad J_z = \chi\frac{(C_{m_F-1}^{+1})^2}{2}|C_1|^2|C_2|^2. \tag{A10}$$

The tunability of $J_\perp$ and J_z is shown in Fig. 2(c). Equation (5) describing the interplay between gravitational redshift and cavity-mediated interactions is a combination of Eqs. (A4) and (A9) in the Wannier-Stark basis.

The physical meaning of the $J_\perp$ term is the spin exchange interactions between $|g, m_F\rangle$ and $|-\rangle$ state via the $\hat{\Pi}^+\hat{\Pi}^-$ process, i.e., an atom in $|-\rangle$ state emits a virtual photon into the cavity and flips to $|g, m_F\rangle$ state ($\hat{\Pi}^-$), and another atom in $|g, m_F\rangle$ state absorbs the same photon and flips to $|-\rangle$ state ($\hat{\Pi}^+$). The physical meaning of J_z term is the collective frequency shift of $|-\rangle$ state via the $\hat{\Sigma}^+\hat{\Sigma}^-$ process, i.e., an atom in $|-\rangle$ state absorbs a photon from the dressing laser beam and emits it into the cavity while staying in the same state ($\hat{\Sigma}^-$), then another atom in $|-\rangle$ state absorbs the same cavity photon and emits it back to the dressing laser beam ($\hat{\Sigma}^+$).

Experimental considerations—Finally, we focus on the experimental requirements of the dressing scheme. For ^{87}Sr atoms, we consider the Zeeman shifts between nuclear spin states to be at the order of 10^2 Hz. In order to frequency resolve a single transition between nuclear spin states, we have $\Omega/2\pi, \delta/2\pi \sim 10$ Hz. Considering $\chi N/2\pi$ at the order of Hz for clock transition as shown

in Ref. [42], and GRS at the order of mHz for 1-cm spatial separation, the validity of the dressing scheme is ensured.

As for experimental implementation, spatial inhomogeneities exist for the atomic frequency and the parameters δ and Ω in E_-. The effects of GRS will be washed out if the inhomogeneities are much larger than the value of GRS. For 1-cm spatial separation, the mHz scale of GRS requires controlling the inhomogeneities below 10^{-4} Hz for direct observation.

For the atomic frequencies and detuning δ, the leading order contributions are from spatial inhomogeneities in the magnetic field. One can suppress first order Zeeman shifts by probing opposite nuclear spin states and calculating the averaged frequency, which is attainable based on the parameters in Ref. [7]. This approach allows for cancellation of first order Zeeman shifts up to shot-to-shot fluctuations, and residue effects of the magnetic field can be distinguished from GRS based on the dressing scheme.

For the dressing laser Rabi frequency Ω, the leading order contributions are from the spatial profile of the laser beam. If we denote the modification of Ω as $\Delta\Omega$, the change of $E_\pm$ is given by

$$\Delta E_\pm/\hbar = \pm\frac{1}{2}\sqrt{\Omega^2+\delta^2}\left(1+\frac{(\Delta\Omega)\Omega}{\Omega^2+\delta^2}\right). \tag{A11}$$

The suppression of inhomogeneities in E_- requires $\Delta\Omega/2\pi < 10^{-4}$ Hz, which is equivalent to $\Delta\Omega/\Omega < 10^{-5}$. In principle, this requirement is achievable using an ultrastable cavity, which allows for precise control of the spatial mode of the dressing laser. Notice that $\Delta E_+ + \Delta E_- = 0$, an alternative approach to reduce this requirement is to average the transition frequency of $|g, m_F\rangle \leftrightarrow |-\rangle$ and $|g, m_F\rangle \leftrightarrow |+\rangle$,

$$\frac{E_-(Z)+E_+(Z)}{2} = \hbar\omega_0 + \frac{\hbar\delta}{2} + \frac{1}{2}\frac{\hbar\omega_0}{c^2}\phi(Z). \tag{A12}$$

In this way, the averaged transition frequency becomes independent of Ω. Even though one sacrifices the full tunability of GRS, it is still changed to half of its value without dressing.